Cleaning of thick viscoplastic surface deposits using an impinging jet

Tuck, Jessica; Alberini, Federico; Ward, Dick; Gore, Bill; Fryer, Peter

DOI:
10.1016/j.jfoodeng.2019.109699

Document Version
Peer reviewed version

Citation for published version (Harvard):
Tuck, J, Alberini, F, Ward, D, Gore, B & Fryer, P 2019, 'Cleaning of thick viscoplastic surface deposits using an impinging jet: effect of process variables ', *Journal of Food Engineering*, vol. 266, 109699. https://doi.org/10.1016/j.jfoodeng.2019.109699

CLEANING OF THICK VISCOPLASTIC SURFACE DEPOSITS USING AN IMPINGING JET: EFFECT OF PROCESS VARIABLES.

Jessica P Tuck[a], Federico Alberini[a],
Dick Ward[b], Bill Gore[b], Peter J Fryer[a]

[a]*School of Chemical Engineering, University of Birmingham, Birmingham B15 2TT, UK*
[b]*Procter and Gamble Corporate Engineering Technical Labs, West Chester, OH, USA*

ABSTRACT

Impinging jets are the tool of choice for cleaning mixing vessels. Layers of product can be left behind on the sides of these vessels. A range of thicknesses in the FMCG industries can be found; thick films are especially difficult to clean. Here data is presented for cleaning thick films (2 - 8 mm) with an impinging water jet. An imaging technique using ultra violet light has been developed to measure cleaning of these thick films as a function of time. Carbopol® 940 solution has been used as a model fluid, representing typical consumer goods, and food products. Cleaning takes place in four stages. For thick film cleaning, there is a delay between impingement and the start of cleaning, in which water is trapped below the deposit to form a blister. The time for the blister to burst was found to be a function of both deposit thickness and nozzle diameter. A stage of rapid cleaning was defined and analysed, with the rate of cleaning here correlating with the flow rate. There was mixed agreement when rapid cleaning data was fitted against previously reported cleaning models for thin films.

1. INTRODUCTION

1.1 Cleaning in Industry

Fouling is a ubiquitous challenge in the fast moving consumer goods (FMCG) and food industries. Process equipment becomes fouled over time, requiring cleaning of both pipework and mixing vessels, each with potentially complex geometries (Friis and Jensen (2016)). Whilst focus on hygienic design can minimise the frequency and intensity of the cleaning process, it cannot eliminate the need for this step (Fryer et al. (2013)). Insufficient cleaning can cause cross contamination of products, poor product quality, or even microbial growth (Lelieveld (2003). Optimising cleaning is essential to reduce the environmental and economic costs of manufacturing.

Cleaning-in-place (CIP) is the use of an automated program to deliver a cleaning regime without dismantling equipment (Tamime (2008)); many CIP programmes have been designed on semi-empirical evidence (Seiberling (2012)). Process vessels can be cleaned by impinging spray devices (Jensen et al. (2011)), commercially available in many designs (for examples see Seiberling and Wish (1959); (Ross, 2016); (Gleeson et al., 2003); (Delaney et al., 2017)). To study vessel cleaning, spray devices are often approximated as a stationary or moving single jet (see Feldung Damkjær et al. (2017), Glover et al. (2016), Morison and Thorpe (2002), and Köhler et al. (2015)).

Fryer and Asteriadou (2009) developed a classification of cleaning processes. Three predominant soil types were identified:

- Type 1 deposit: Viscous products which clean with the mechanical action of water flow alone.
- Type 2 deposit: Biofilms which require both biocides and the mechanical action of water flow.
- Type 3 deposit: Cohesive solids requiring both chemical and mechanical action for removal.

Type 1 deposits include foods, toothpastes and cosmetic creams, which can be viscous non-Newtonian fluids that are difficult to remove, and produce fouling layers that both fill pipework, and form millimetre to centimetre thick layers on vessel walls. Palabiyik et al. (2018) correlated the cleaning time, t, of a series of Type 1 materials with different yield stresses. Commonly a number of different products are made on the same plant. The need

during product changeover is first to remove as much product as possible and then clean the rest as quickly as possible.

1.2 Cleaning with Impinging jets

The behaviour of an impinging jet on a clean surface has been extensively studied (for example by Watson (1964); Nakoryakov et al. (1978); and Olsson and Turkdogan (1966)). When a vertical water jet hits a horizontal surface a hydraulic jump can be observed at some radius, in which the fast flowing thin film, greatly reduces in velocity and increases in depth. For a water jet hitting a non-horizontal wall, the oblique impingement angle causes this pattern to become asymmetric (Kate et al. (2007)). Following the terminology of Wang et al. (2013) the thin, fast flowing area is referred to as the radial flow zone, which reaches a film jump, comparable to the hydraulic jump. Morison and Thorpe (2002) studied the wetting rate, Γ, of a single water jet, equation (1), was shown to correlate the cleaning effect of the jet.

$$\Gamma = \frac{\dot{m}}{W} \tag{1}$$

Where ṁ is the mass flow rate of the jet, and W is the width of the wetted surface.

Wilson et al. (2012) continued the work of Morison and Thorpe (2002), studying the surface flow and drainage of an impinging jet. In this work a model describing the radius of the radial flow zone, R, was defined by:

$$R = 0.276\left[\frac{\dot{m}^3}{\mu\rho\gamma(1-\cos\beta)}\right]^{\frac{1}{4}} \tag{2}$$

Where β is the contact angle of the jet substrate on the impinged surface, μ is the dynamic viscosity of the jet fluid, ρ is the density of the jet fluid, and γ is the surface tension. This model balances the jet momentum with the surface tension in the film. Bhagat et al. (2018) provided further validation of this model.

1.3 Models for cleaning thin films

Yeckel and Middleman (1987) studied the removal of deposit by the shearing force of an impinging jet, and developed a model for the cleaning of thin films, an order of magnitude thinner than the water flow above it. Yeckel and Middleman (1987) approximated the shearing forces for a jet running over a clean surface to develop their model. Whilst their

model was effective at predicting cleaning over longer periods of time, it was not accurate in the initial cleaning stage.

Wilson et al. (2014) applied the momentum balance of Wilson et al. (2012), to products cleaned by adhesive removal. In these experiments, thin layer of polyvinyl acetate (PVA) (δ = 70 - 140 ± 30 μm), Xanthan gum (δ = 80 μm), and petroleum jelly (δ = 250 - 300 ±30 μm) were investigated. A linear relationship between the radius of the cleaned zone, r_c, and time, t, was defined by:

$$r_c \approx \sqrt[5]{\frac{3k'}{\pi c}\dot{m}^3}(t - t_i)^{\frac{1}{5}} = K\Delta t^{0.2} \quad (3)$$

Where k' is a lumped cleaning rate constant, a function of the deposit properties, K is a lumped cleaning rate parameter, and t_i is the time at which a circular cleaning pattern was first observed. There was good agreement between the cleaning rate of each soil material and the model, when the cleaning area was confined to the radial flow zone. The cleaning of hydrophobic petroleum jelly was studied at varying temperatures, and shown to fit equation 3, which further validated the momentum based model. When measuring cleaning against time for petroleum jelly, the cleaning profiles, plotted in the form suggested by Equation 3, initially follows a linear trend, before the rate of cleaning drops as it appears to reach a plateau. This linear region was isolated when fitting the petroleum jelly data to equation 3, which gave a good fit.

Glover et al. (2016) developed the Wilson et al. (2014) model, investigating k', as a function of deposit thickness, δ, and deposit type. In this work two complex deposits were studied:

(i) Water based PVA (δ_{dry} = 20 μm -170 μm), swelled on contact with the water jet and was removed by peeling, which in the first stages of cleaning lead to a non-circular cleaned area. K was found to be independent of thickness.

(ii) Petroleum jelly (δ = 50 μm – 2000 μm), showed variability in cleaning dependant on the application method. This product had a yield stress, τ_y = 50 Pa. K was found to decrease for increasing layer thickness. The area cleaned to a plateau value, which was modelled as a balance between the jet momentum and soil strength.

The models of Wilson and co-workers demonstrate good agreement with the cleaning of thin surfaces, and are of wide applicability. The cleaning of a thick film (of thickness > 2 mm) has

however previously been largely unreported. Some data shown in Tuck et al. (2019) suggested mechanistic differences between thin and thick film removal for Carbopol dispersed in water and cosmetic cream. Here these differences are discussed in much greater detail, by studying the removal of films up to 8 mm thick.

2. Experimental Techniques and Methods

2.1 Apparatus

Experiments used the set-up shown schematically in Figure 1. A centrifugal pump (Cole-Palmer Micropump®), was used to supply water at 470 ml min^{-1} - 1140 ml min^{-1}, from a supply tank. Birmingham City tap water at 20 °C was used for the impinging water jet. Three fabricated circular pipe nozzles (20 mm in length), with inner diameters, d_i, 1 mm, 1.5 mm, and 2 mm were inserted into tubing (d_i = 5 mm) connected to the pump. The nozzle was secured to provide a stationary vertical jet, 40 mm (± 1 mm) from the test surface. This jet length, L, ensured the water jet was coherent at the point of impingement, with $L < L_c$, where L_c is the jet length at which instabilities first occur, as described in Middleman (1995). The jet conditions used in this work are laid out in Table 1.

The test surface was raised and angled at 30° from the horizontal, to allow for detached deposit and water to be displaced from the point of impingement. This ensured the downstream conditions did not affect the testing area. Kate et al. (2007) give equations for film thickness away from the impingement point; for nozzles between 1 – 2 mm these equations give a film thickness of 35 – 120 μm, at a radius 2 mm from the impingement point, significantly smaller than the deposit thicknesses.

Deposit was applied to a standardized test surface, a stainless steel plate uniformly coated in matte black spray paint. This coating was required to minimise reflections, allowing for adequate visualisation necessary for the visualisation technique. Between experiments the test surface was cleaned using cold water as not to disrupt the coating, and dried before a new layer of deposit was applied.

2.2 Materials

Carbopol® 940 (as supplied by Lubrizol) dispersed in water was selected as the model deposit. Carbopol is a common component (as carbomer) in many industrial fluids (Baki (2015)). The rheological properties of Carbopol 940 are subject both to its concentration in water, and the pH of the solution, are widely published, for example Barry and Meyer (1979), R. Varges et al. (2019), Alberini et al. (2014). For these results a mixture of Carbopol 940 (0.2 wt. %) in deionized water was used. Due to its low wettability, the Carbopol 940 powder was slowly added to the water, and this solution was left to stir for ~ 12 h. A commercial

available UV reactive cosmetic paint (UV glow purchased from amazon.com) was used as a luminescing agent. This luminescing agent was determined to be effective at a concentration of 0.9 g L^{-1}, this was then added to the Carbopol solution and left to stir for ~ 2 h. Once a homogeneous solution had formed, NaOH was slowly added to increase the pH of the gel to pH 4.5, which increased the viscosity, and yield stress of the material into the desirable range.

Rheological properties were measured using a flow sweep performed at room temperature, measured using cone and plate geometry (60 mm, 2°), on a TA Instruments AR 1000 Rheometer (Figure 2). Following previous findings, the yield stress, $\tau_{y,}$ of the deposit was measured by fitting a Herschel-Bulkley model to these results (Alberini et al. (2014)). The yield stress, τ_y, for the Carbopol solution with the addition of the UV paint, τ_y was averaged at 3 Pa.

For these experiments a 2, 4, or 8 mm thick layer of deposit was used. Carbopol was applied to the test surface by pouring the gel into a fabricated template, dimensions (70 mm x 100 mm x 2 - 8 mm thickness), with excess gel being removed. The method ensured a consistent and even layer of deposit.

2.3 Experimental Technique

Using the experimental set up shown in Figure 1, a method was developed to capture the rate of cleaning. To measure cleaning, images were captured with the camera, which was set to image the hard surface whilst the deposit was cleaned. Commercially available UV lamps were used to illuminate the test surface, with the luminescence from the doped Carbopol deposit captured by the camera. Images were recorded at 50 - 60 frames per second, and analysed by a MATLAB® algorithm that converts each of the frames into a grey scale image. The luminescing deposit shows as bright pixels on the images, corresponding to a high grey level. Once the deposit is cleaned, the non-reflective hard surface shows as a dark spot, giving a low grey level. The program is written allowing a threshold to be set, designating pixels with a high grey level as ‘unclean’, and pixels with a low grey scale value as clean. The images were recorded in 8-bit giving 256 grey levels.

Figure 3(a) shows a sample histogram depicting the frequency of pixels for each grey level, for the image of a partially cleaned surface shown in Figure 3(b). Analysis of the raw images, as demonstrated by the labelled pixels in Figure 3(b), suggests that the cluster of peaks below

grey scale 15 depict the partially cleaned, and cleaned areas. In this work clean is defined as visually clean, therefore the partially cleaned pixels were not defined as clean, only pixels with the value 10 and below. The value of the threshold depended on the lighting used and in practice varied between 8 – 20, depending on the individual case. Each experiment contained a ruler in frame, allowing for the scale to be set for each run (≈ 0.1 mm pixel^{-1}), so that the clean pixel count can be converted into an area. The algorithm thus gives a value of cleaned area, A_c, for each frame of a known time after impingement, t. An example of the results produced for a single experiment (δ = 2 mm, d_i = 1 mm, Q = 600 ml min^{-1}) using this method, is shown in Figure 4(a). For clarity, every third data point is plotted here with each data point corresponding to the analysis of a single frame. The repeatability of the technique is shown in Figure 4(b) which depicts results for 4 individual experiments with the same conditions (δ = 2 mm, d_i = 1 mm, Q = 600 ml min^{-1}). Minor differences between runs can be observed with the overall cleaning values, whilst the shape of the cleaning profile remains significantly similar for all the trials. The average absolute deviation for Figure 4(b), is 25 mm^2, 2% of the average cleaned area at 4 s. Experiments were concluded either after 5 seconds or when the cleaned area reached the edge of the plate.

3. Results and Discussion

3.1 Cleaning mechanisms of thin and thick films

The cleaning mechanism of a thin film, defined here as $\delta \leq 2$ mm, has been described in Wilson et al. (2014), in terms of a clean area expanding from the point of impingement. This behaviour is depicted by the results shown in Figure 4(a) for 2 mm thick films. An immediate cleaned area is produced on jet impingement, together with an initially rapid rate of cleaning which decreases over time. The insert to Figure 4(a) shows the cleaned area (black) at points a-d on the curve. It can be seen that cleaned area is seen and can be measured from 0.1s after impingement (point a). Glover et al. (2016) described that in results for rheologically complex materials, cleaning approached an asymptote related to the material yield stress.

In contrast, Figure 5 shows the cleaning profile for a thick film ($\delta = 8$ mm). More complex behaviour is seen than for thinner films. On the left hand side of Figure 5 are four sample images from which the data points were derived from, labelled a - d. The first notable difference from the thin film, is the delay of approximately 0.6 s before the start of cleaning. After this delay, rapid cleaning occurs followed by a plateau starting at approximately 1.4 s.

Figure 6 includes a schematic illustration of the stages highlighted in Figure 5. These are visualised from both a view parallel to the plate, and also as a cut through, showing the profile of the deposit at the point of impingement. Cleaning takes place in four stages:

I. *Jet impingement*: the impinging jet impacts the deposit, disrupting the cohesive bonds within the material, to pierce through to the hard surface (data not shown).

II. *Blister formation*: water spreads under the deposit, breaking adhesive bonds between the deposit and the hard surface. During this period the cohesive bonds surrounding this suspended layer of deposit remain intact, holding the deposit in place. This gives minimal disruption to the deposit surface, so no visually cleaned area is produced during this step.

III. *Blister burst*: the cohesive bonds give way to the pressure of the increasing volume of water trapped between the hard surface and deposit material. During this step rapid cleaning is observed, between images (b) and (d).

IV. *Perimeter cleaning*: after the blister bursts, cleaning proceeds slowly. The deposit around the perimeter of the original burst area is slowly eroded, giving a slight increase in the radius of the cleaned area. Cleaning has a minimal impact due to water flowing away from the cleaned area over unremoved deposit.

Figure 7 compares typical variations of cleaned areas for a thin (2 mm) and thick (8 mm) film, highlighting also the differences between cleaning mechanisms. While cleaning of thick films is characterised by the four stages previously defined (see Figure 5), the cleaning of thin films only exhibits two stages, a rapid cleaning phase and a falling rate stage, which can be considered analogous to stages III and IV, respectively, in thick films.

To quantify rapid cleaning in both cases, the start and end points for this stage were identified as follows, and shown in Figure *7*:

(i) The time at which blister formation ends and rapid cleaning begins in thick films was defined as the blister burst time, t_b. Given the initial fluctuations in cleaned areas for thick films (see Figure 7 inset), t_b was defined as the time taken to reach a cleaned area of 50 mm^2 (dashed line in Figure 7). This value was chosen to give a true representation of when the blister bursting begins, observed on the raw images, and is much larger than the area recorded during blister formation. For comparison, t_b - i.e. time taken to clean an initial area of 50 mm^2 – was also considered as the start point of rapid cleaning in thin films, also shown in Figure 7.

(ii) In thick films, the end of the rapid cleaning period was identified through the change in the slope of the cleaning curve that marks the transition from the blister burst to the perimeter cleaning stage (e.g. stages II, ca. 0.6s and IV, ca. 1.4s, respectively in Figure 5). Analogously, the rapid cleaning end point in thin films was defined by the slope change that marks the beginning of the falling rate stage. A built-in MATLAB® function (findchangepts) was used to analyse cleaned area experimental data and identify those slope changes, locating the transition points robustly, and marking the end of the rapid cleaning phase. The transition points for the conditions shown in Figure 7, are denoted by grey circles for each cleaning curve, and labelled A_t.

3.2 Effect of thickness and flow rate

Figure 8 shows the cleaning profiles for δ = 2 mm films, cleaned by water jets with varying nozzle sizes (1-2 mm) and flow rates (500- 1140 ml min^{-1}). The results show the area cleaned, which is an oval due to the slope of the plate. Each line is the average of 4 experiments repeated with the same conditions. The instant start in cleaning, at t = 0, suggesting thin film behaviour, is observed for each of the conditions measured. This is followed by rapid cleaning over the first second after impingement, followed by a reducing

cleaning rate. This cleaning profile is seen for all conditions, with the flow parameters affecting both the rate of cleaning and the magnitude of the cleaned area.

In the first half second the cleaning rate for all flow conditions is the same independent of flow rate and nozzle size. Divergence between cases occurs after approximately 0.5 s, at this point cleaning curves diverge into three, one for each nozzle size. It is not until almost 1 s that the results for different flow rate within each nozzle size diverge from each other. This suggests that nozzle size rather than flow rate affects the first second of cleaning, perhaps as the nozzle size determines the size of the entry hole created in the jet impingement stage. Within two seconds the cleaning rate slows, with the sharpest transition shown for the 2 mm nozzle size.

Table 2 presents data for the cleaned area at selected time points from Figure 8, highlighting the effects of nozzle size and flow rate during the thin film cleaning process. Table 2 compares the results for the conditions ($Q = 715$ ml min^{-1} with $d_i = 1.0$ mm and $d_i = 1.5$ mm, and $Q = 1060$ ml min^{-1} for $d_i = 1.5$ mm with $Q = 1140$ ml min^{-1} for $d_i = 2.0$ mm). After 1 and 2 s, the cleaned areas vary between nozzle sizes, with the larger nozzle sizes producing the larger cleaned area. After three seconds however, the cleaned areas are within 10 % of each other for comparable flow rates, and at four seconds the results have almost converged. These results again highlight the greater effect of nozzle size over the first stages of cleaning, after which the effect of flow rate dominates the magnitude of the cleaned area.

Figure 9 shows results for a fixed nozzle size $d_i = 1.5$ mm, but for a range of flow rates, and two film thicknesses, $\delta = 2$, and 4 mm. Two distinct mechanisms can be observed: for 2 mm films, cleaning begins at once, whilst, each of the 4 mm experiments show a delay of approximately 0.4 s before cleaning begins. This suggests a transition between $\delta = 2$ and 4 mm, between thin to thick film (blister formation) behaviour, for this rheology. After three seconds, the cleaned areas for $\delta = 4$ mm are between 73 – 77% of those recorded for the same flow conditions and 2 mm thickness.

As seen in Figure 8, for each thickness flow rate appears to have minimal effect on the rate and extent of cleaning in the first stages of the process. The impact of flow rate is observed at approximately 0.8 s and 1.1 s for the $\delta = 2$ mm, and $\delta = 4$ mm respectively. As there is about 0.4 s delay before cleaning is seen for the $\delta = 4$ mm films, the effect of flow rate is seen after a comparable time of rapid cleaning for both film thicknesses. This suggests that for the first second in cleaning, whilst deposit thickness has a large impact, flow rate has less effect under

the conditions used here. In optimising cleaning, therefore, these results suggest that it will be useful to know what the thickness of a residual layer of deposit will be.

Further demonstration of thickness effects is shown in Figure 10, which demonstrates the effect of thickness for a single flow condition (d_i = 2 mm, Q = 1140 ml min^{-1}), but for film thickness of 2, 4 and 8 mm thick. As shown in previous figures, a delay in cleaning is observed for both δ = 4 mm, and δ = 8 mm, indicating thick film (blister formation) behaviour, with the delay in the 8 mm film being longer than that for the 4 mm film. As observed in Figure 9, at any time the amount of surface cleaned decreases with film thickness.

3.3 Fit to Established Kinetic Models

Equation (3) from (Wilson et al., 2014) has previously been used to model data. To compare this model with the current data set the data was cropped to only include the rapid cleaning phase, i.e. to remove the blister formation and perimeter cleaning stages of the cleaning process from the analysis. We thus define Δt in equation (3) as the time from the start of the rapid cleaning phase ie, area cleaned > 50 mm^2. To average the data, the blister burst time, t_b, was set to t = 0 for each individual experiment, and four individual experiments were then averaged between t = 0 and the end of the rapid cleaning phase determined by the MATLAB® function described earlier (and shown in Figure 7). If necessary, the data was further cropped to the length of the shortest data set; i.e. using the experiment with the shortest rapid cleaning phase observed. In the subsequent figures, the radius r_c in equation 3 was taken as a nominal radius $\sqrt{(A_c/\pi)}$, where A_c is the removed area measured by the protocol of section 2.3. This is an approximation given that the cleaned area was an oval.

Figure 11 shows the 'the rapid cleaning phase' of each of the jet parameters shown in Figure 8, represented as described in equation 3. Portions of the results follow a linear trend as predicted by equation (3), whilst there is separation between data obtained for nozzle sizes. The average of the R^2 terms of results shown in Figure 11 when fitted as a linear model were, d_i = 1 mm R^2 = 0.966 ± 0.005, d_i = 1.5 mm R^2 = 0.937 ± 0.018, d_i = 2 mm R^2 = 0.944.

In Figure 12 data for the intermediate (4 mm thick) and thick (8 mm thick) films are shown. Each graph depicts a single flow rate and thickness, with varied nozzle sizes, and show some straight-line behaviour. The analysis that leads to equation (3) gives k' as a parameter

describing product type and product thickness, with the overall constant K being a function of both k' and mass flow, with no effect of nozzle size. Here the product type was kept constant, so that K should be a function of only product thickness and mass flow. The K values identified from in Figure 12 are laid out in Table 3. The data is averaged for all nozzle sizes; the standard deviations of K increases for thicker films, suggesting nozzle diameter may influence K. Larger K values were observed for the thinner film as expected, with a more significant decrease with thickness for the lower flow rate.

The data suggests that the analysis of Wilson et al. (2014) can be applied to thick films here, albeit only for the region of rapid cleaning. There is a greater effect of nozzle size than expected from the model, but less dependence than in the initial stages of cleaning up to the blister burst time.

An extended data set is shown in the Appendix, in Appendix 1 the cleaning profiles for 18 conditions are shown, highlighting the cleaning behaviour of 4 mm and 8 mm thick films as functions of flow rate, and nozzle size. Appendix 2 contains the same experimental data as Appendix 1, however it is presented as in Figure 11, modelling the results from Wilson 2014. These extended data sets highlight the complexities of thick film cleaning. It does appear, however, that equation (3) does not apply to the thick films examined here, and that further work is needed.

3.4 Analysis of whole data set

The blister burst time, t_b, is a previously unreported parameter, seen only in thick film cleaning. In Figure 13 the blister burst time, t_b, is plotted against the nozzle diameter. The data is highly scattered, but a relationship can be observed for $\delta = 8$ mm, with a marginal decrease in time, with the increase in nozzle size. The standard deviation of the data also decreased with nozzle size, from 0.355 s to 0.098 s, giving more repeatable results. This suggests a recommendation of a larger nozzle size to decrease the delay before cleaning begins. Evaluation of t_b, as a function of flow rate, Reynolds number, and velocity, found no useful fit to data (not shown here).

Isolating the region where the blister bursts, causing rapid cleaning, marked as region III in Figure 5, allowed a constant cleaning during this crucial stage to be evaluated. Figure 14 shows the relationship between this rate of cleaning and the flow rate of the impinging jet.

There does appear, particularly at lower flow rates, to be an overall positive correlation between the rate of cleaning observed and the flow rate. All three film thicknesses are shown here which contributes to some of the increased scatter. The correlation measured between the rapid cleaning rate and the flow rate varied with each thickness (δ = 2 mm, R^2 = 0.782; δ = 4 mm, R^2 = 0.718; δ = 8 mm, R^2 = 0.660); the data is scattered, with the correlation getting worse with increasing thickness. When a straight line is plotted for data for the same thickness of deposit, the slope of the line (defined here as K') obtained from this graph varies with thickness (δ = 2 mm, K' = 121 mm^2 ml^{-1}; δ = 4 mm, K' = 133 mm^2 ml^{-1}; δ = 8 mm, K' = 102 mm^2 ml^{-1}), with an overall K' = 127 mm^2 ml^{-1}. No cleaning data was obtained for flow rates below 470 ml min^{-1}: but the data suggests very low cleaning rates would occur at those values.

4 CONCLUSIONS

Cleaning of deposits from tanks and pipework is a major contributor to the waste created in a process plant. Cleaning of 2 – 8 mm thick layers of Carbopol 940 deposit was performed with a coherent impinging water jet. A bench scale rig was developed and used to study and quantify the cleaning mechanisms of thick films. The cleaning was measured using a UV imaging technique, using a MATLAB® script to measure individual pixels in each image taken during the cleaning process. These pixels were then classified as clean or dirty dependant on their grey scale value, giving a value for the cleaned area in each image, at a known time after impingement.

Previous published work by Wilson and co-authors has defined the cleaning behaviour of thin films. Data on the cleaning of 2 mm thin film showed agreement with previous work; there is an immediate start in cleaning, and after a rapid cleaning phase, the rate of cleaning reduces to a plateau value. Thick film cleaning shows more complex behaviour; cleaning occurs in four stages; (i) Jet impingement as fluid first contacts the deposit and penetrates it; (ii) Blister formation: liquid then spreads out underneath the deposit creating a raised blister that disturbs the deposit surface but does not give any cleaned surface for periods of up to seconds; (iii) Blister burst, the blister bursts, creating a rapidly increase in the cleaned area, leaving (iv) Perimeter cleaning of a near-circular area that cleans slowly.

Previous models of cleaning have suggested that only jet mass flow rate has an effect; in this work however some effect of jet thickness (different nozzle diameter) was seen. The time at which the blister burst was defined and measured for the thick films, and found to be a slight function of nozzle diameter. The cleaning rate, starting at the time the blister bursts, and ending before the perimeter cleaning, was also measured, and showed a linear relationship with flow rate, with variability between the differing thicknesses. Some of the cleaning behaviour fitted the type of equation defined by Wilson and co-workers. The dynamics of the interaction between the flow and the deposit is more complex than for thin films; work is ongoing to identify the critical factors that affect the cleaning rate.

5 ACKNOWLEDGEMENTS

We would like to gratefully acknowledge Procter and Gamble, and Engineering and Physical Sciences Research Council for financially supporting this research though the EPSRC CDT in Formulation Engineering (EP/L015153/1). We wish to acknowledge assistance with the MATLAB® function from Dr Estefanía López Quiroga.

Nomenclature

Roman

A_c: area cleaned, mm^2

A_t: area cleaned at transition, mm^2

c: lumped parameter, $kg^2\ m^{-4}\ s^{-1}$

d_i: nozzle inner diameter, mm

k: consistency index, $Pa\ s^{n-1}$

k': lumped cleaning rate constant, $m\ s\ kg^{-1}$

K: gradient of cleaning profile plots, $m\ s^{-0.2}$

K' slope of the straight line fitted to the data of Figure 14, $mm^2\ ml^{-1}$

L: distance from nozzle to impact on surface, m

L_c: coherent length, m

$\dot{m}$: mass flow rate in jet, $kg\ s^{-1}$

n: flow behaviour index, dimensionless

Q: flow rate, $L\ h^{-1}$

R: radius of film jump, m

r_c: radial co-ordinate, m

t: time, s

Δt: total time after cleaning front is first seen, $= t - t_i$, s

t_i: time at which cleaning front is first seen, s

t_b: blister burst time, s

W: wetted width, m

Greek

β: contact angle, °

γ: surface tension (liquid/vapour), $N\ m^{-1}$

δ: deposit thickness, m

μ: dynamic viscosity, Pa s

ρ: density, kg m^{-3}

τ_y: deposit yield stress, Pa

Γ: wetting rate, kg m^{-1} s^{-1}

Acronyms

CIP: cleaning in place

FMCG: fast moving consumer goods

PVA: polyvinyl acetate

UV: ultraviolet

ALBERINI, F., SIMMONS, M. J. H., INGRAM, A. & STITT, E. H. 2014. Use of an areal distribution of mixing intensity to describe blending of non-newtonian fluids in a kenics KM static mixer using PLIF. *AIChE Journal,* 60**,** 332-342.

BAKI, G. 2015. *Introduction to cosmetic formulation and technology / Gabriella Bak and Kenneth S. Alexander*, Hoboken, New Jersey : Wiley, 2015.

BARRY, B. W. & MEYER, M. C. 1979. The rheological properties of carbopol gels I. Continuous shear and creep properties of carbopol gels. *International Journal of Pharmaceutics,* 2**,** 1-25.

BHAGAT, R. K., JHA, N. K., LINDEN, P. F. & WILSON, D. I. 2018. On the origin of the circular hydraulic jump in a thin liquid film. *Journal of Fluid Mechanics,* 851**,** R5.

DELANEY, R. E., DELANEY, A. K., MARCH III, J. H., MORGAN, C. & STEWART, G. E. 2017. Rotary impingement cleaning device with replaceable cartridge gear train. Google Patents.

FELDUNG DAMKJÆR, N., ADLER-NISSEN, J., JENSEN, B. B. B. & WILSON, D. I. 2017. Flow pattern and cleaning performance of a stationary liquid jet operating at conditions relevant for industrial tank cleaning. *Food and Bioproducts Processing.*

FRIIS, A. & JENSEN, B. B. B. 2016. Chapter 18 - The Hygienic Design of Closed Equipment. *In:* LELIEVELD, H., HOLAH, J. & GABRIĆ, D. (eds.) *Handbook of Hygiene Control in the Food Industry (Second Edition).* San Diego: Woodhead Publishing.

FRYER, P. J. & ASTERIADOU, K. 2009. A prototype cleaning map: A classification of industrial cleaning processes. *Trends in Food Science & Technology,* 20**,** 255-262.

FRYER, P. J., ROBBINS, P. T. & ASTERIADOU, I. K. 2013. Current Knowledge in Hygienic Design: Can We Minimise Fouling and Speed Cleaning? *In:* YANNIOTIS, S., TAOUKIS, P., STOFOROS, N. G. & KARATHANOS, V. T. (eds.) *Advances in Food Process Engineering Research and Applications.* Boston, MA: Springer US.

GLEESON, B. F., DELANEY, A. K., LE, M. Q. & DELANEY, R. E. 2003. Cleaning apparatus especially adapted for cleaning vessels used for sanitary products, and method of using same. Google Patents.

GLOVER, H. W., BRASS, T., BHAGAT, R. K., DAVIDSON, J. F., PRATT, L. & WILSON, D. I. 2016. Cleaning of complex soil layers on vertical walls by fixed and moving impinging liquid jets. *Journal of Food Engineering,* 178**,** 95-109.

JENSEN, B., NIELSEN, J., FALSTER-HANSEN, H. & LINDHOLM, K. 2011. Tank cleaning technology: innovative application to improve clean-in-place (CIP). *EHEDG Yearbook,* 2012**,** 26-30.

KATE, R. P., DAS, P. K. & CHAKRABORTY, S. 2007. Hydraulic jumps due to oblique impingement of circular liquid jets on a flat horizontal surface. *Journal of Fluid Mechanics,* 573**,** 247-263.

KÖHLER, H., STOYE, H., MAUERMANN, M., WEYRAUCH, T. & MAJSCHAK, J.-P. 2015. How to assess cleaning? Evaluating the cleaning performance of moving impinging jets. *Food and Bioproducts Processing,* 93**,** 327-332.

LELIEVELD, H. L. M. 2003. Hygiene in food processing / edited by H.L.M. Lelieveld ... [et al.]. Cambridge: Cambridge : Woodhead.

MIDDLEMAN, S. 1995. 4 - The transitions from drops to a coherent jet and back to drops. *Modeling Axisymmetric Flows.* San Diego: Academic Press.

MORISON, K. R. & THORPE, R. J. 2002. Liquid Distribution from Cleaning-in-Place Sprayballs. *Food and Bioproducts Processing,* 80**,** 270-275.

NAKORYAKOV, V. E., POKUSAEV, B. G. & TROYAN, E. N. 1978. Impingement of an axisymmetric liquid jet on a barrier. *International Journal of Heat and Mass Transfer,* 21**,** 1175-1184.

OLSSON, R. G. & TURKDOGAN, E. T. 1966. Radial Spread of a Liquid Stream on a Horizontal Plate. *Nature,* 211**,** 813-816.

PALABIYIK, I., LOPEZ-QUIROGA, E., ROBBINS, P. T., GOODE, K. R. & FRYER, P. J. 2018. Removal of yield-stress fluids from pipework using water. *AIChE Journal,* 64**,** 1517-1527.

R. VARGES, P., M. COSTA, C., S. FONSECA, B., F. NACCACHE, M. & DE SOUZA MENDES, P. R. 2019. Rheological Characterization of Carbopol® Dispersions in Water and in Water/Glycerol Solutions. *Fluids,* 4**,** 3.

ROSS, M. 2016. Device for cleaning closed spaces. Google Patents.

SEIBERLING, D. A. 2012. Appendix B - Tank Cleaning. *In:* HALL, S. (ed.) *Branan's Rules of Thumb for Chemical Engineers (Fifth Edition).* Oxford: Butterworth-Heinemann.

SEIBERLING, D. A. & WISH, F. W. 1959. Spray nozzle for liquid storage tanks. US Patent 2,895,688.

TAMIME, A. Y. 2008. Cleaning-in place : dairy, food and beverage operations / edited by Adnan Tamime. 3rd ed. ed. Oxford: Oxford : Blackwell.

TUCK, J. P., ALBERINI, F., WARD, D., GORE, B. & FRYER, P. J. 2019. Cleaning of thick films using liquid jets. *Energy Procedia,* 161**,** 93-99.

WANG, T., FARIA, D., STEVENS, L. J., TAN, J. S. C., DAVIDSON, J. F. & WILSON, D. I. 2013. Flow patterns and draining films created by horizontal and inclined coherent water jets impinging on vertical walls. *Chemical Engineering Science,* 102**,** 585-601.

WATSON, E. J. 1964. The radial spread of a liquid jet over a horizontal plane. *Journal of Fluid Mechanics,* 20**,** 481-499.

WILSON, D. I., ATKINSON, P., KÖHLER, H., MAUERMANN, M., STOYE, H., SUDDABY, K., WANG, T., DAVIDSON, J. F. & MAJSCHAK, J. P. 2014. Cleaning of soft-solid soil layers on vertical and horizontal surfaces by stationary coherent impinging liquid jets. *Chemical Engineering Science,* 109**,** 183-196.

WILSON, D. I., LE, B. L., DAO, H. D. A., LAI, K. Y., MORISON, K. R. & DAVIDSON, J. F. 2012. Surface flow and drainage films created by horizontal impinging liquid jets. *Chemical Engineering Science,* 68**,** 449-460.

YECKEL, A and MIDDLEMAN, S. 1987. Removal of a viscous film from a rigid plane surface by an impinging liquid jet. *Chemical Engineering Communications,* 50, 165-175

Flow rate ($ml.min^{-1}$)	Nozzle size (m)	Mean Velocity ($m.s^{-1}$)	Nozzle Reynolds Number
470	0.001	9.97	9940
600	0.001	12.7	12700
715	0.001	15.2	15100
860	0.001	18.2	18200
600	0.0015	5.66	8460
715	0.0015	6.74	10100
865	0.0015	8.16	12200
1060	0.0015	10.0	15000
600	0.002	3.18	6350
865	0.002	4.59	9150
1140	0.002	6.05	12100

Table 1: Data for the water jet conditions used in this work.

d_i (mm)	Flow Rate ($ml.min^{-1}$)	Area at 1 s	Area at 2 s	Area at 3 s	Area at 4 s
1.0	715	677	1080	1360	1580
1.5	715	954	1300	1480	1620
1.5	1060	1160	1950	2400	2690
2.0	1140	1670	2230	2540	2730

Table 2: Data from Figure 8 describing the cleaned area of 2 mm thick films for varying flow parameters. The cleaned area at selected time points, for conditions with different nozzle sizes yet similar flow rates, have been highlighted here.

Figure	Flow Rate ($ml.min^{-1}$)	Thickness (mm)	K ($mm.s^{0.2}$)	Standard Deviation ($mm.s^{0.2}$)
12a	600	4	14.6	2.39
12b	865	4	25.3	4.81
12c	600	8	9.20	10.7
12d	865	8	21.4	5.69

Table 3: Data from Figure 12, listing the overall K coefficient, defined in equation 3, averaged over multiple nozzle diameters, at fixed flow rates and thicknesses.

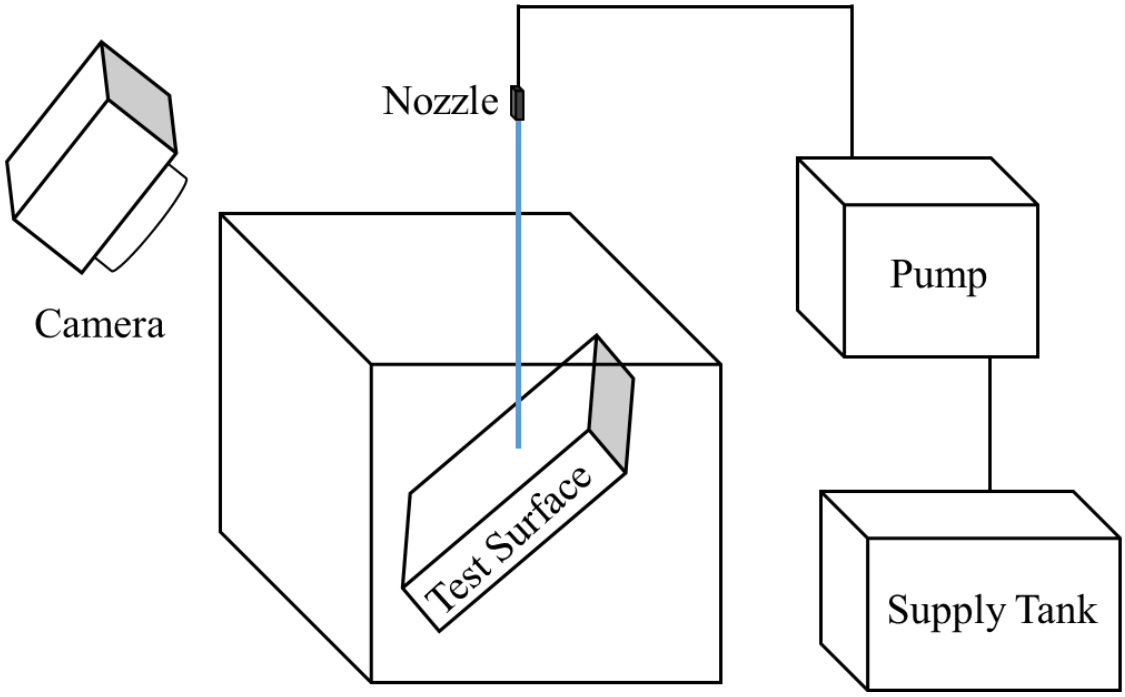

Figure 1: Schematic depicting the bench scale sized experimental test rig.

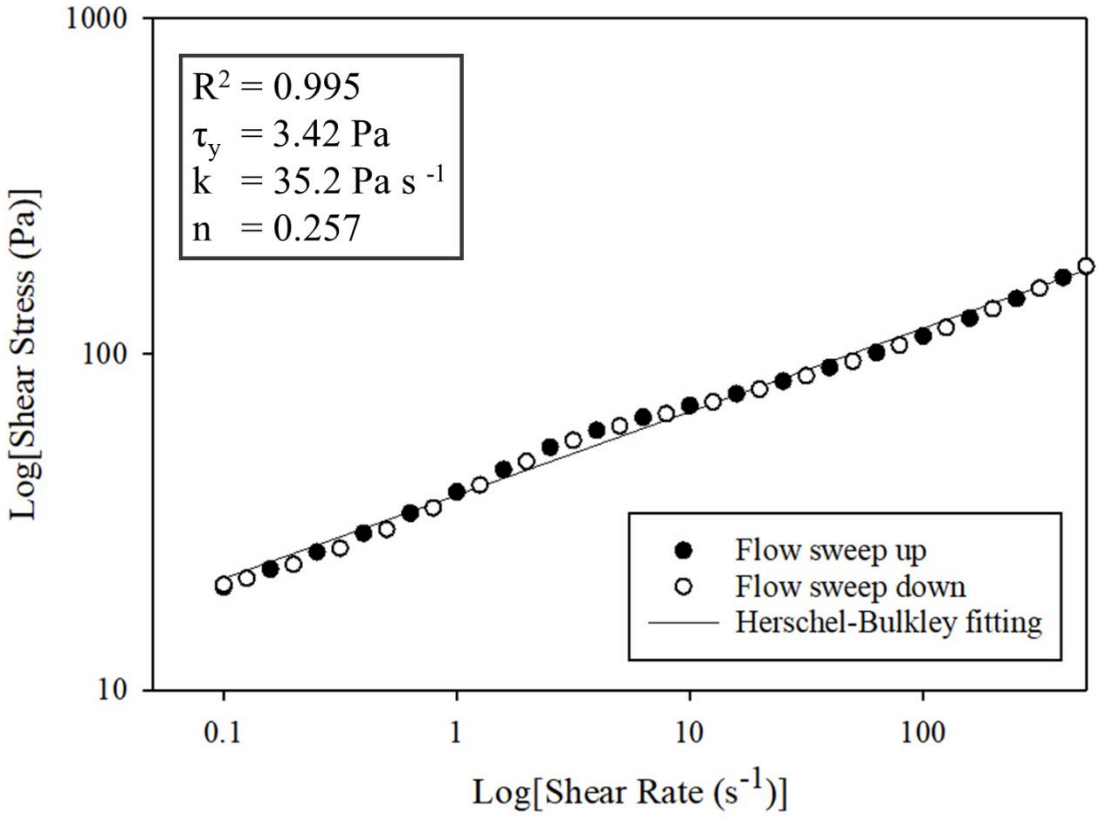

Figure 2: Flow sweep results (from 0.1 – 500 s^{-1}) for the Carbopol deposit, showing shear thinning behaviour. The Herschel-Bulkley fitting is for the flow sweep up, with the corresponding values shown inset.

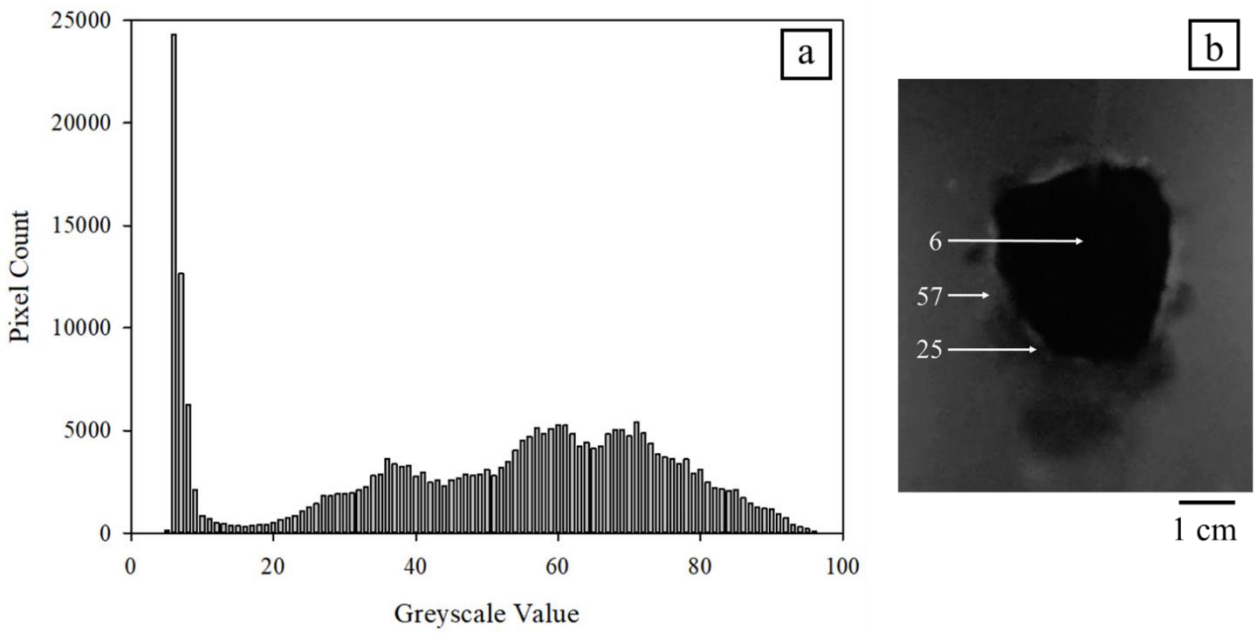

Figure 3: A histogram plotting the grey scale values against the pixel count for the example image shown to the right. This example image was chosen to show a portion of partially cleaned deposit, so the values of the clean, and dirty pixels could be established. The greyscale values for various portions of the image are labelled. The separation between 'cleaned' and 'uncleaned' area is set at 10.

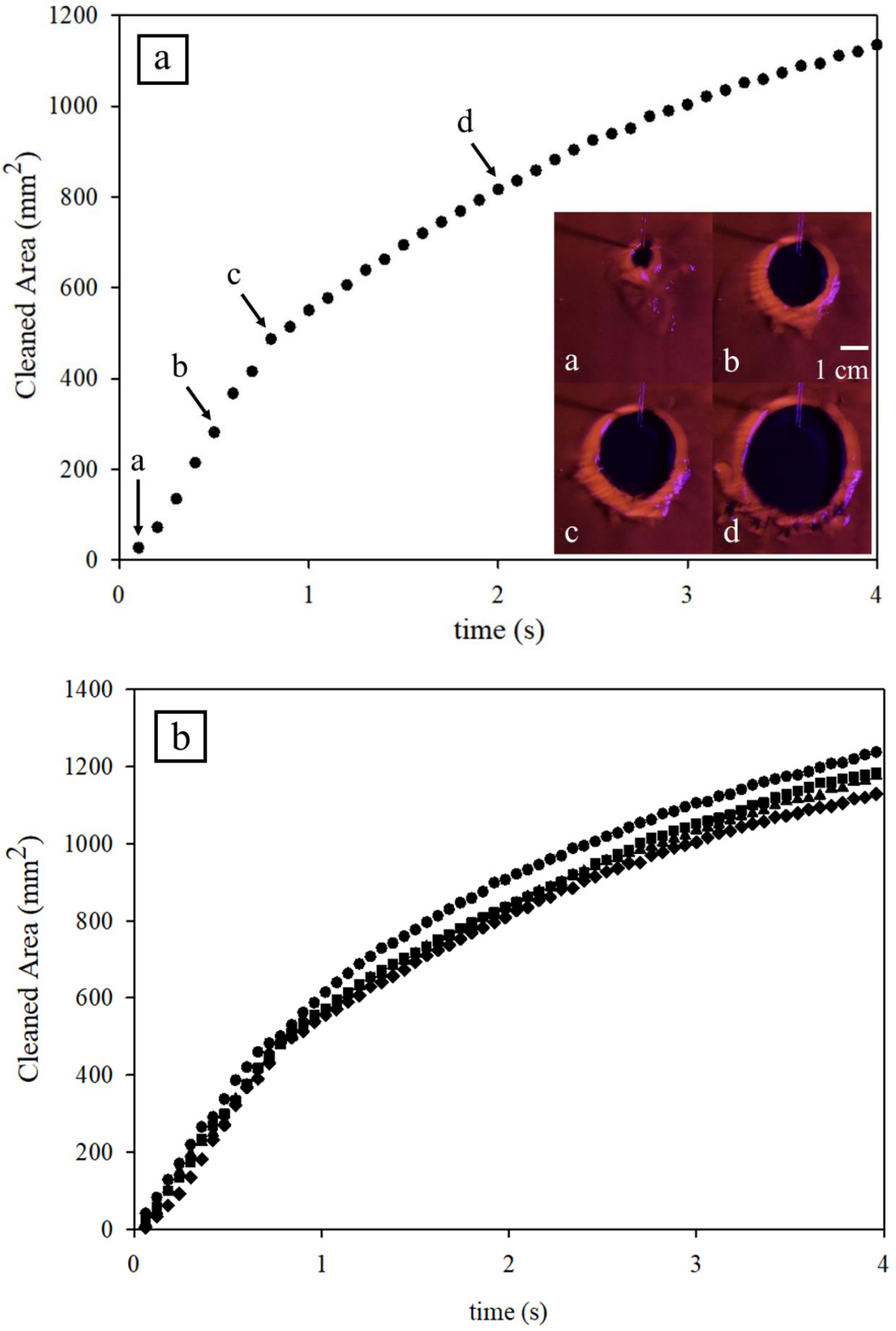

Figure 4: (a) Results for a single experiment, with every third data point shown. Here a thin film (δ = 2 mm) was cleaned by an impinging water jet (Q = 600 ml min^{-1}, d_i = 1.0 mm). At the side the raw images are shown labelled with their corresponding data point. (b) Results for each of the four experiments performed for the parameters Q = 600 ml min^{-1}, d_i = 1.0 mm. Showing the reliability of the experimental set up and technique.

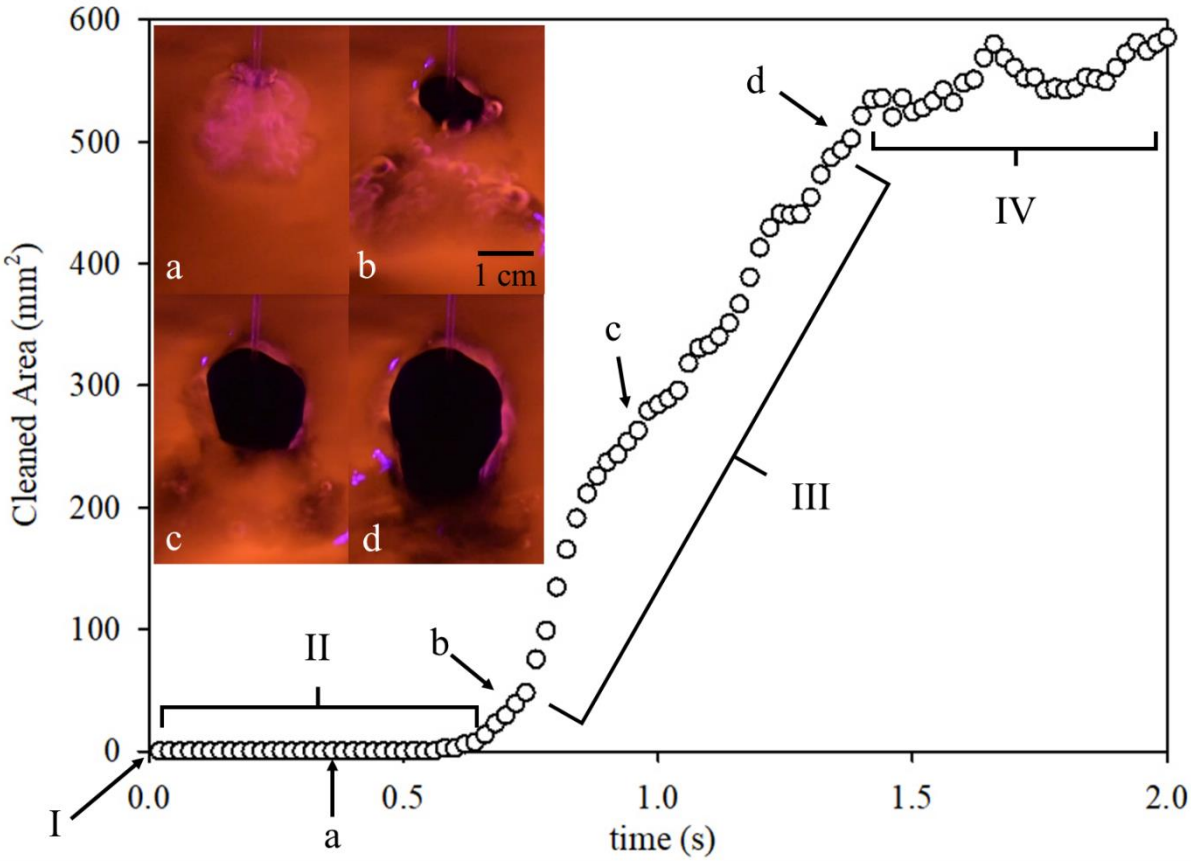

Figure 5: Graph showing results for a single cleaning experiment (Q = 715 ml min^{-1}, d_i = 1.0 mm). At the side the raw images are shown labelled with their corresponding data point. The stages I - IV are those listed in the text. Images (a – d) were taken at the times shown.

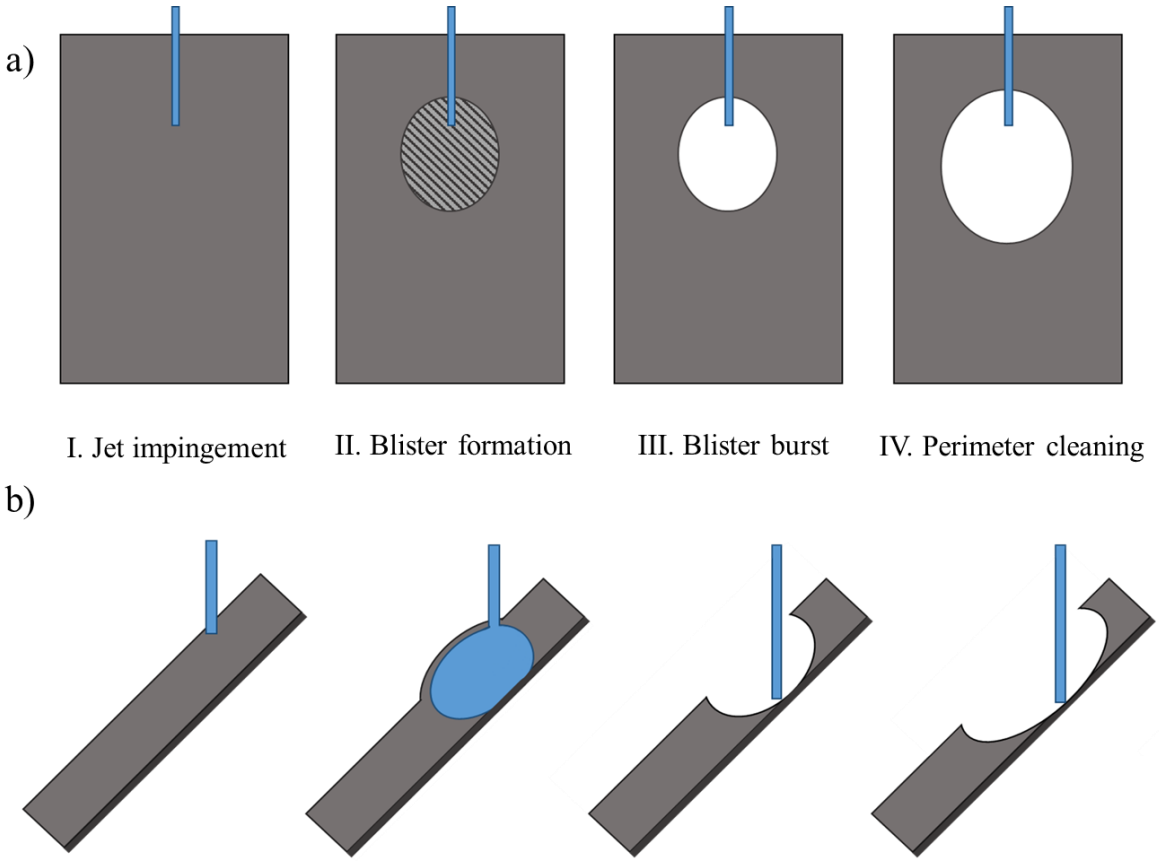

Figure 6: The stages of cleaning for thick films, illustrated from a) plan view normal to the impact plate b) a cross-sectional side view. The corresponding data points, and zones are shown in Figure 5.

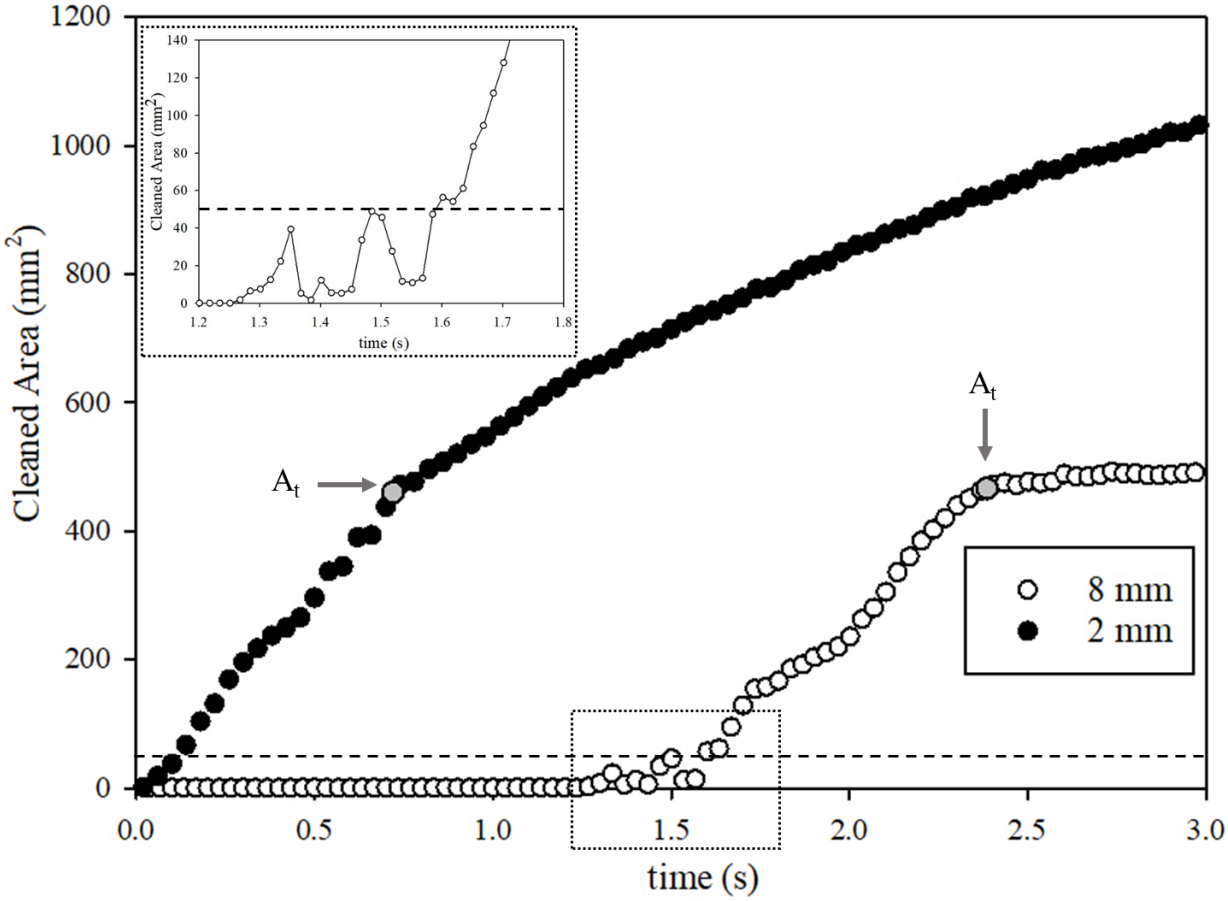

Figure 7: Showing the cleaned area over time for 2 mm and 8 mm thick films cleaned by a water jet (Q = 470 ml min^{-1}, d_i = 1 mm). The horizontal dashed line indicates A_c = 50 mm^2, defined here as the point of the blister burst time. The grey points highlight the end of the rapid cleaning phase (the area cleaned at transition, A_t) as defined by the MATLAB script in section 3. Inset shows an expanded view of the point at which t_b is defined.

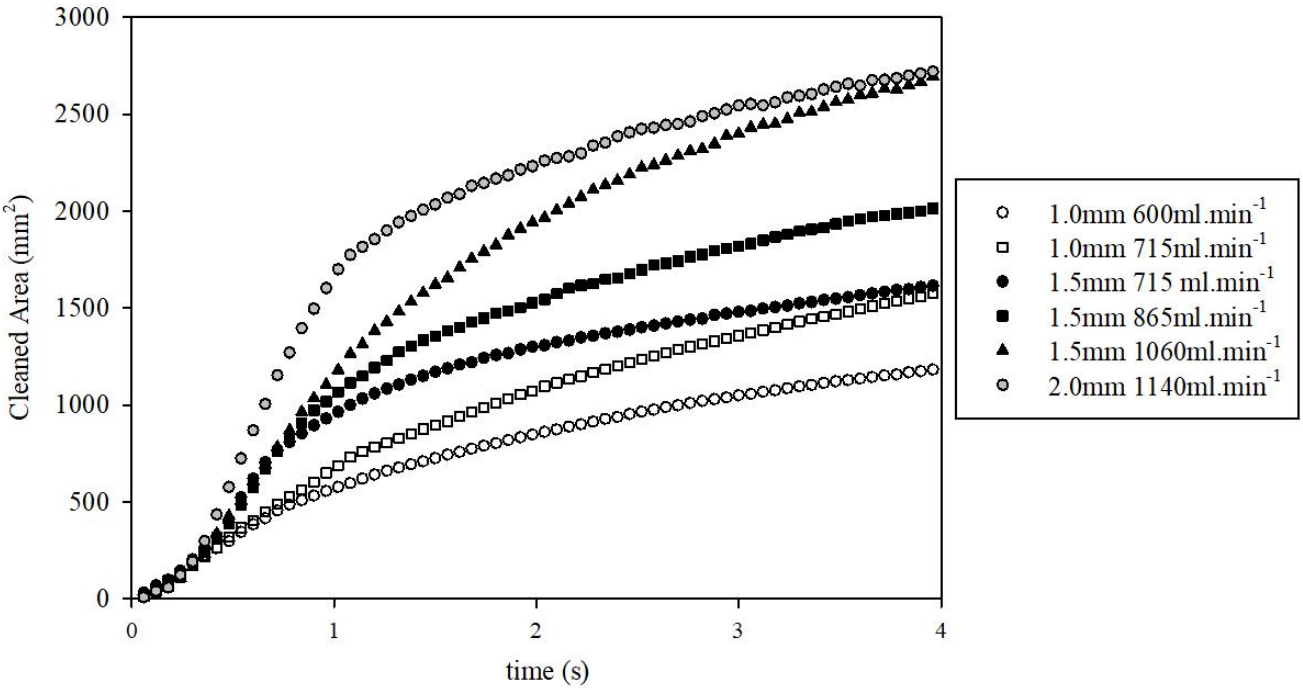

Figure 8: Cleaning profiles for thin film deposits δ = 2 mm, showing the area cleaned for the first 4 s after jet impingement.

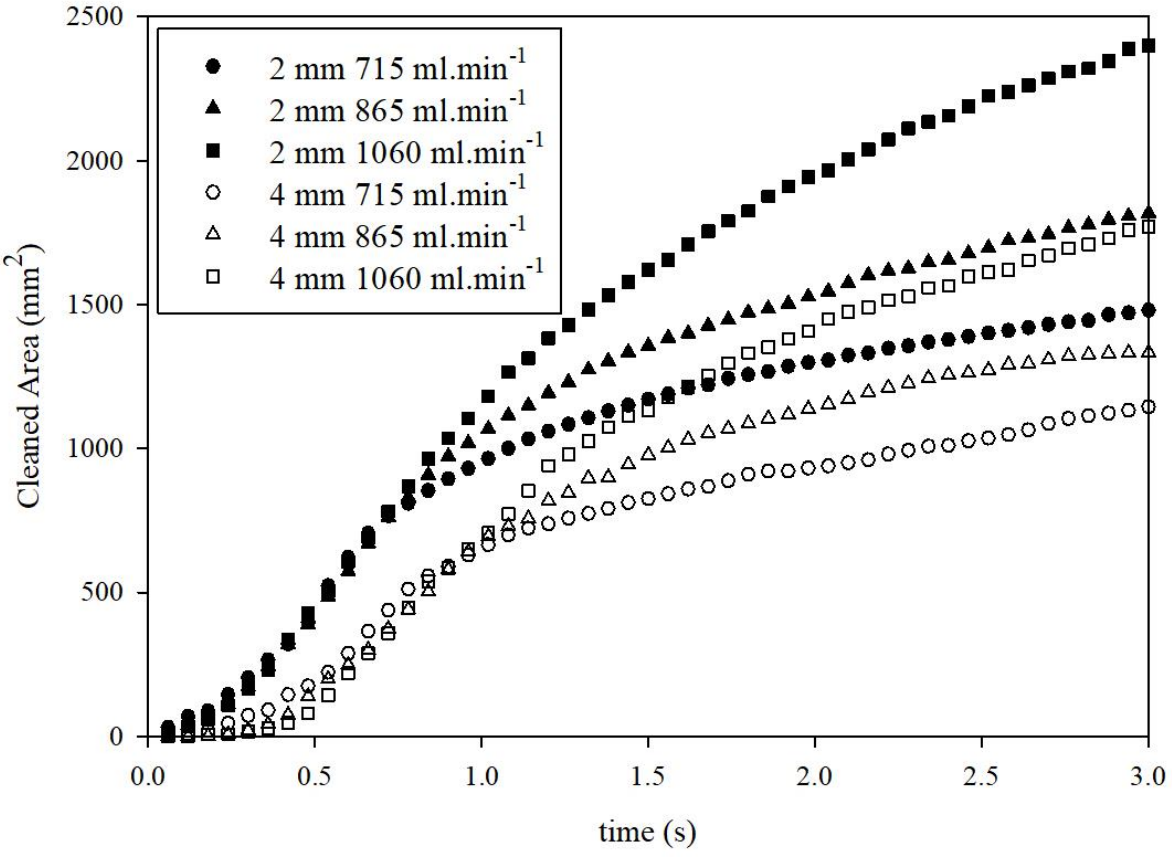

Figure 9: Cleaning profiles for a fixed nozzle size (d_i = 1.5 mm), whilst varying the thickness and flow rate.

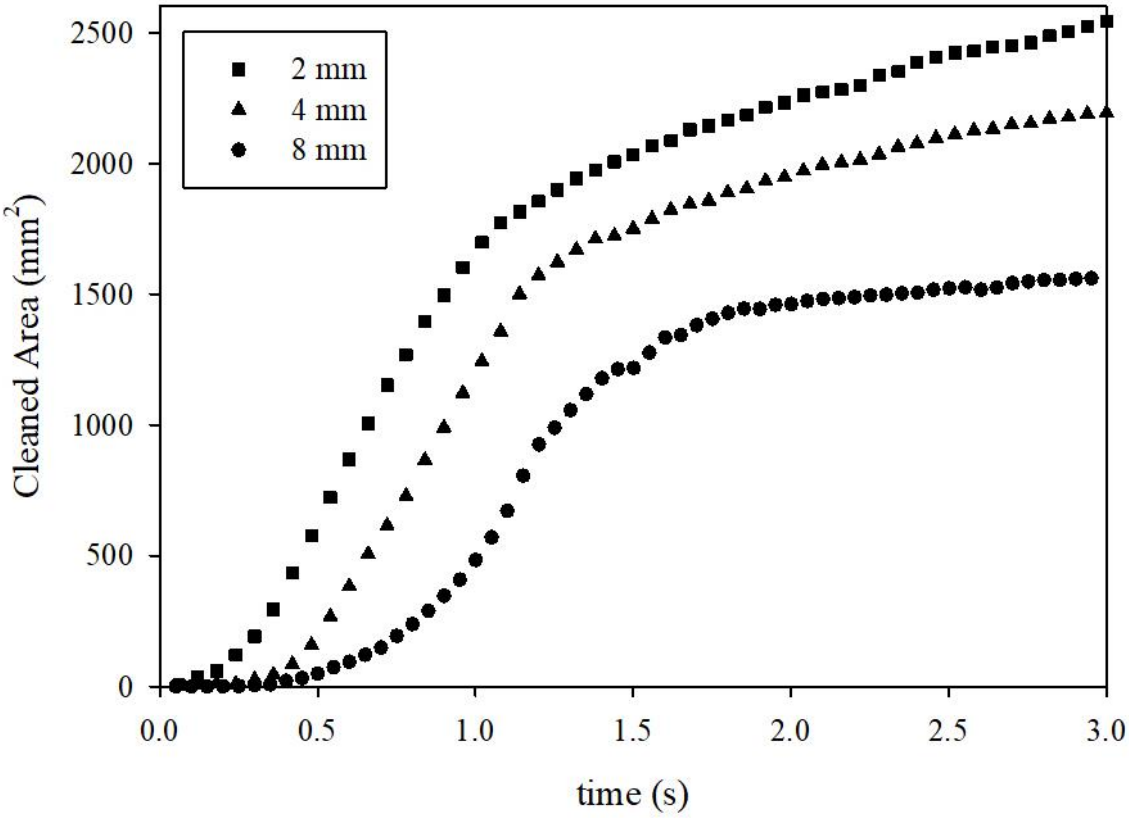

Figure 10: Cleaning profile highlighting the effect of thickness for a single flow condition (d_i = 2 mm, Q = 1140 ml min^{-1})

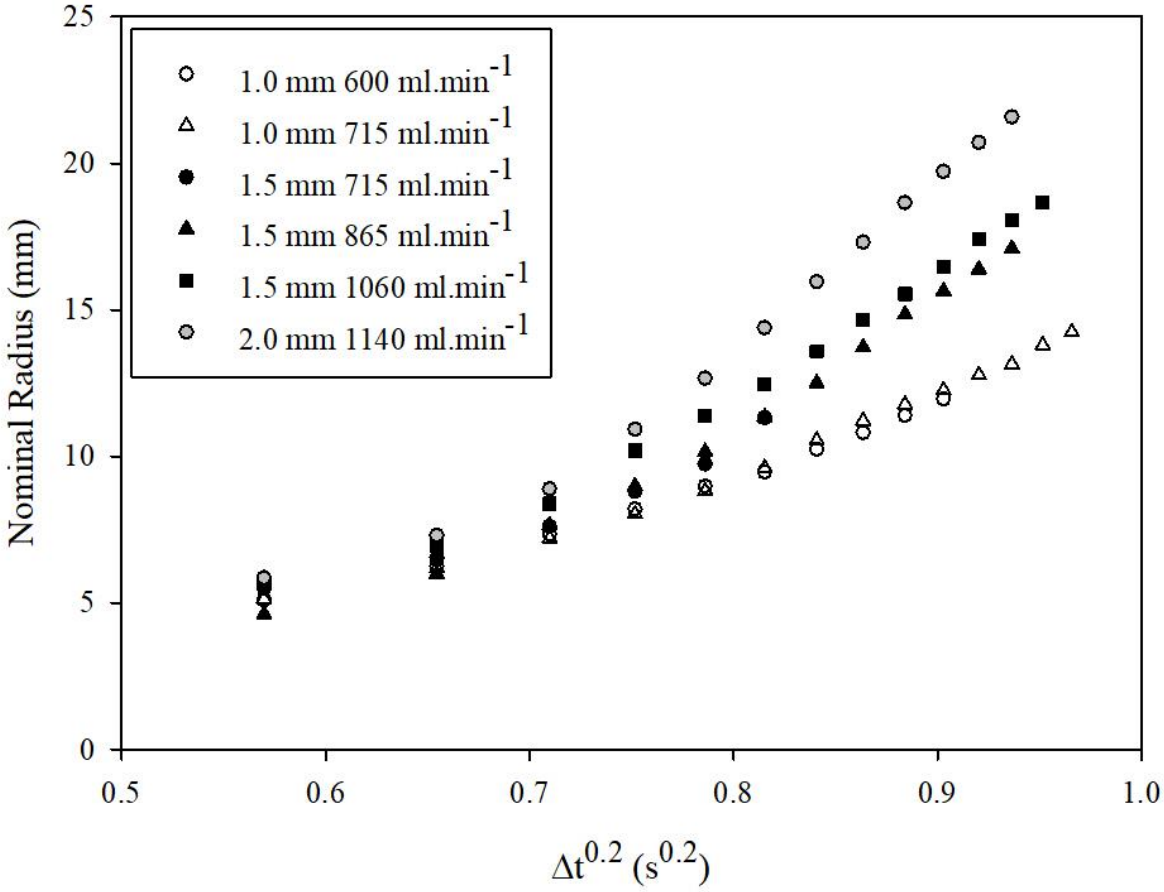

Figure 11: Results for thin film deposits δ = 2 mm, when modelled as a nominal radius against time$^{0.2}$, as previously reported in Wilson 2014. The data here has been cropped to include only the rapid cleaning phase as highlighted in Figure 7, section 3, i.e. region III of the cleaning curve, bounded by the start point (50 mm^2), and the end of the rapid cleaning region.

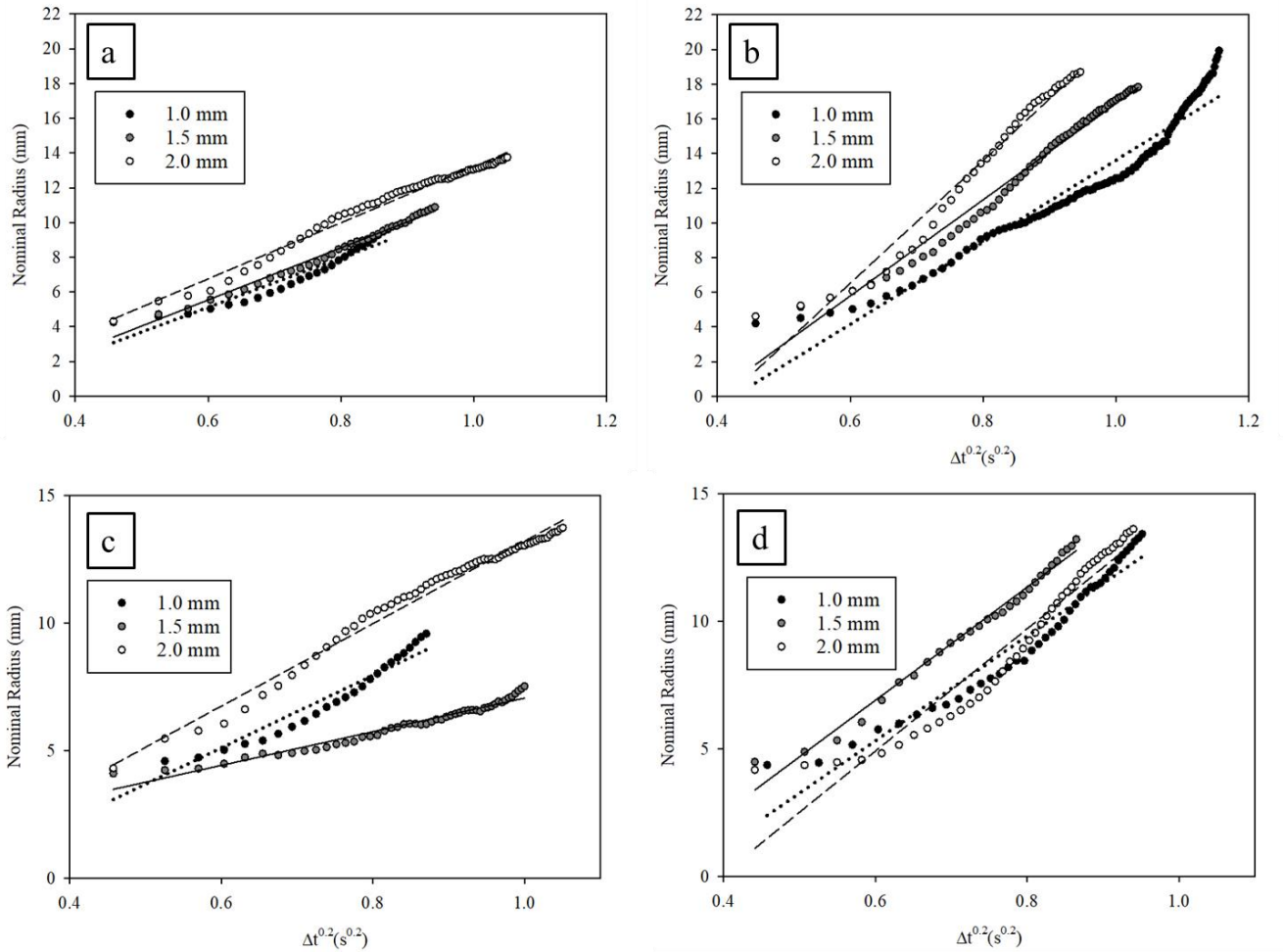

Figure 12: Figures showing experiments with the same mass flow but varying nozzle sizes. The lines of best fit have been included, dotted line corresponds to d_i = 1.0 mm, solid line corresponds to d_i = 1.5 mm, and dashed line corresponds to d_i = 2.0 mm. a) δ = 4 mm, Q = 600 ml min^{-1} b) δ = 4 mm, Q = 865 ml min^{-1} c) δ = 8 mm, Q = 600 ml min^{-1} d) δ = 8 mm, Q = 865 ml min^{-1}

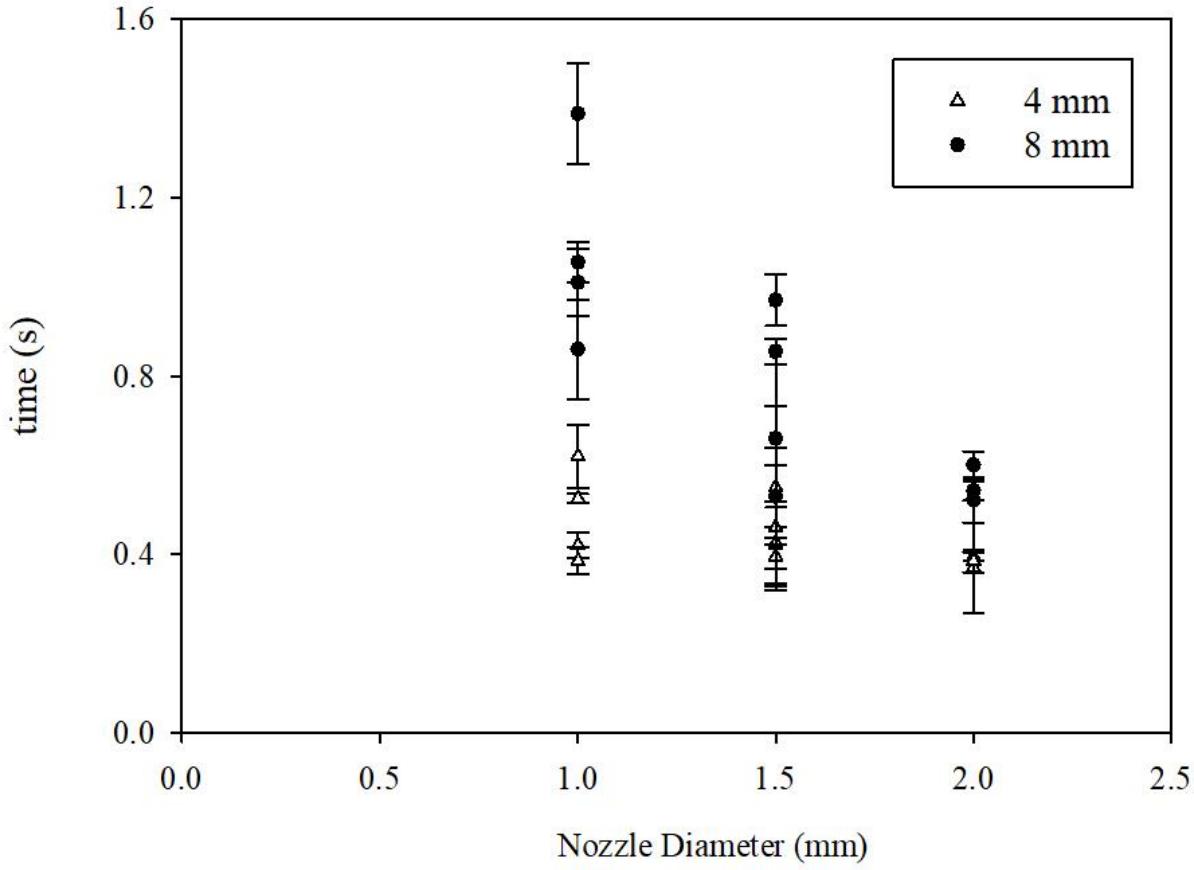

554

555 Figure 13: The relationship between nozzle size and the time at which blister bursts, t_b,
556 defined by the method discussed in Section 3 (i.e area = 50mm^2).

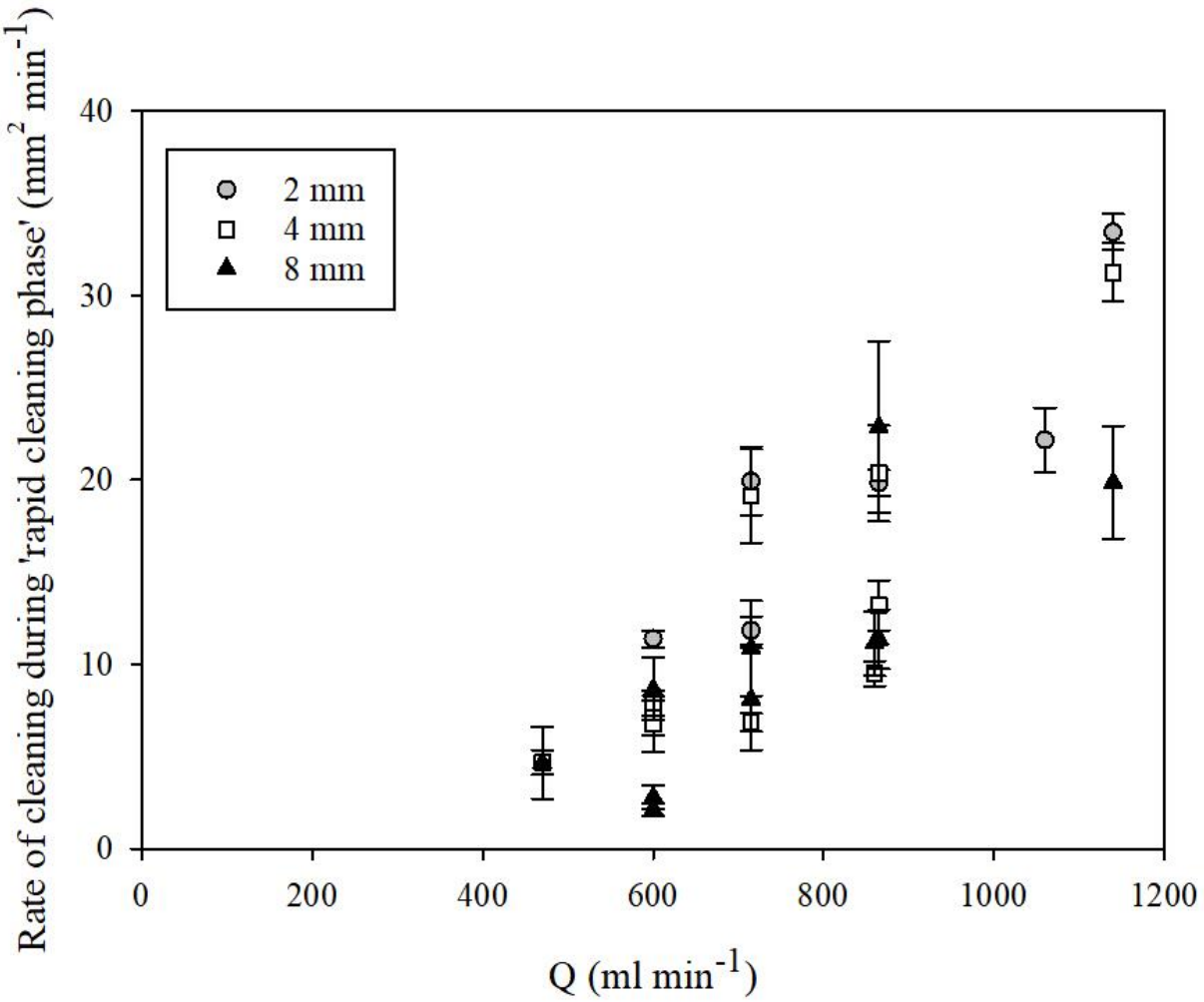

557

558 Figure 14: The relationship between the rate of cleaning during the defined 'rapid cleaning
559 phase' and the flow rate of the impinging jet, as a function of nozzle size.

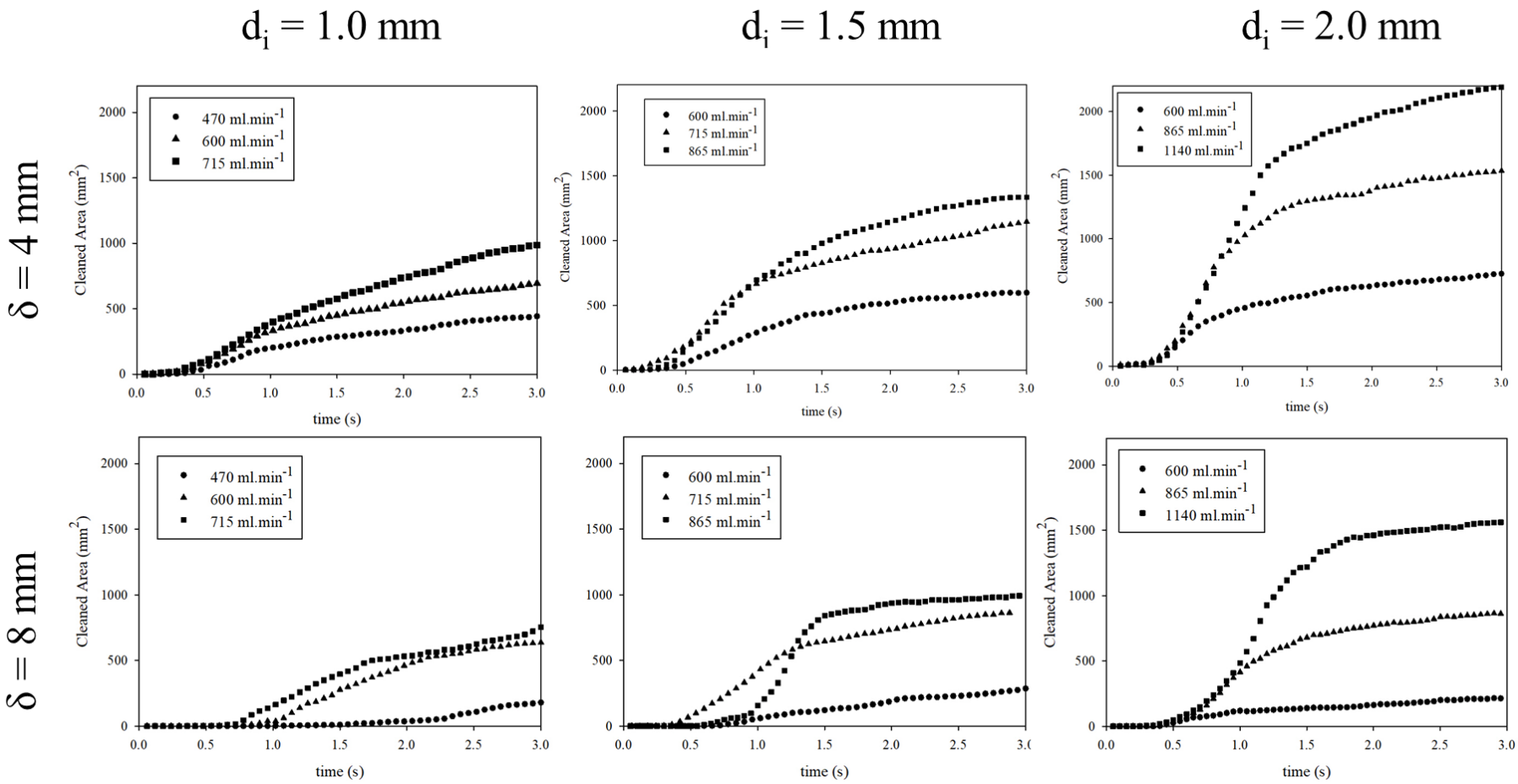

Appendix 1: Extended example results showing the cleaning profiles for a selection of parameters. Cleaning profiles for δ = 4 mm on the top row, and δ = 8 mm for the bottom row, separated into nozzle sizes.

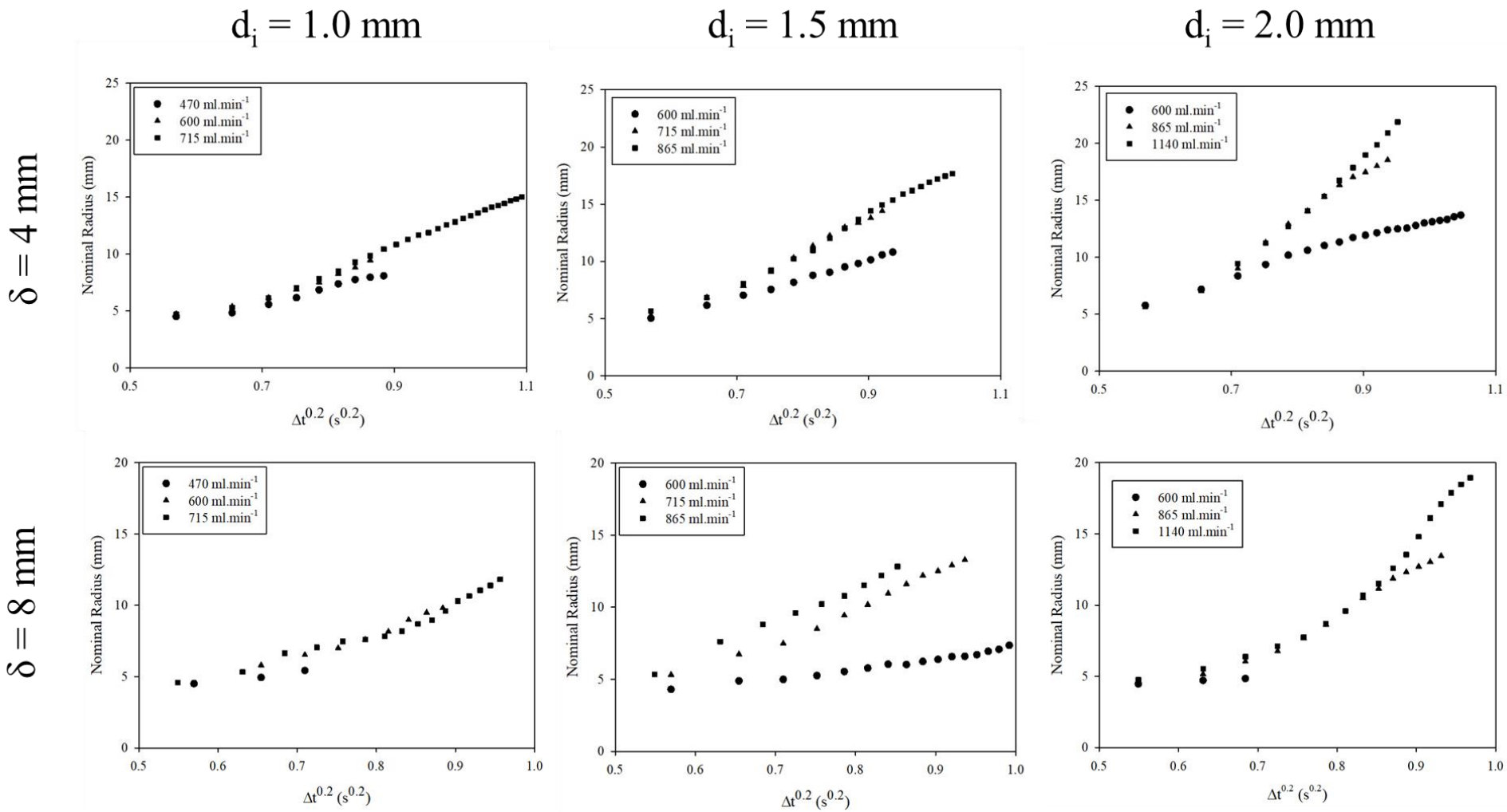

Appendix 2: Extended selection of results which model the results shown in Wilson et al. (2014). Results for δ = 4 mm on the top row, and δ = 8 mm for the bottom row, separated into nozzle sizes.